Theoretical Considerations of Tissue Electroporation With High-Frequency Bipolar Pulses

Christopher B. Arena, Michael B. Sano, Marissa Nichole Rylander, and Rafael V. Davalos*, *Member, IEEE*

***Abstract*—This study introduces the use of high-frequency pulsed electric fields for tissue electroporation. Through the development of finite element models and the use of analytical techniques, electroporation with rectangular, bipolar pulses is investigated. The electric field and temperature distribution along with the associated transmembrane potential development are considered in a heterogeneous skin fold geometry. Results indicate that switching polarity on the nanosecond scale near the charging time of plasma membranes can greatly improve treatment outcomes in heterogeneous tissues. Specifically, high-frequency fields ranging from 500 kHz to 1 MHz are best suited to penetrate epithelial layers without inducing significant Joule heating, and cause electroporation in underlying cells.**

***Index Terms*—Bipolar pulses, electroporation, nanosecond pulsed electric field, oscillating electric field, transmembrane potential.**

I. Introduction

ELECTROPORATION is a nonlinear, biophysical mechanism in which the application of an external pulsed electric field leads to an increase in the permeability of cellular membranes. While direct evidence for the exact mechanism of electroporation has yet to be discovered [1], early *in vitro* experiments suggest that the extent of electroporation is attributed to the induced buildup of charge across the plasma membrane, and consequently, transmembrane potential (TMP) [2]–[7]. The applied field strength and pulse duration control the TMP development and the extent to which transient permeabilizing defects are allowed to reseal. If the pulse parameters are tuned such that the membrane defects are only temporary, and the cell remains viable, the process is termed reversible electroporation. Reversible electroporation can be used to introduce molecules into cells that, under normal conditions, would not permeate cellular membranes [8]. Irreversible electroporation (IRE) results when membrane defects are irrecoverable, leading to cell death presumably through a loss of homeostasis [9], [10]. Recently, electroporation has been utilized *in vivo* as a means to destroy cancer cells within tissues in both reversible and irreversible modalities. Reversible electroporation is being studied to facilitate the delivery of anticancer drugs and DNA into cancer cells through the plasma membrane in the form of electrochemotherapy (ECT) and electrogenetherapy (EGT), respectively. IRE promotes cell necrosis [11] and is an independent means to destroy substantial volumes of targeted tissue without the use of harmful adjuvant chemicals, if used prior to the onset of thermal injury [12].

Common protocols for IRE, ECT, and EGT involve delivering multiple, unipolar pulses with a duration on the order of microseconds through electrodes inserted directly into, or adjacent to, the malignant tissue [12]–[15]. When the tumor is located deep within an organ, a minimally invasive needle or catheter-based device is needed for the electrodes to reach the tumor. In some instances, the organ puncture required by these designs can, in itself, damage the surrounding healthy cells [16], [17]. There is also the possibility of reseeding cancer cells upon device removal. Therefore, the use of nonpuncturing plate electrodes placed around the organ is desirable in some instances. Plate electrodes are best suited to treat tumors lying close to the skin, because a high potential drop occurs across the skin, where the field is the largest, limiting the amount of deeper tissue that can be permeabilized without first permeabilizing the skin [14], [15]. However, the high electric field in the skin can lead to deleterious thermal damage through the mechanism of Joule heating [18]. Plate electrodes will have similar problems when placed around internal organs to treat tumors. Most organs are covered by the peritoneum, where the presence of tight junctions concentrates the field across epithelial cells, because extracellular current pathways are reduced [19]. We hypothesize that these problems can be mitigated by implementing high-frequency bursts of bipolar pulses with a burst width on the order of microseconds and a duration of single polarity on the order of nanoseconds.

To the best of our knowledge, the benefits of bipolar pulses have only been studied for electroporation applications at the single-cell level. Theoretically, Talele *et al*. have shown that asymmetrical electroporation due to the resting TMP ($\sim$0.1 V) [20] of cells seen when unipolar pulses are delivered [21], [22] can be alleviated by switching to bipolar pulses [23]. Experimentally, this leads to increased efficiency of macromolecule uptake through the membrane [21], [22]. Depending on the extracellular conductivity, bipolar pulses with a frequency of 1 MHz (i.e., 500 ns duration of single polarity) can also lessen

Manuscript received October 2, 2010; revised November 22, 2010; accepted December 15, 2010. Date of publication December 23, 2010; date of current version April 20, 2011. This work was supported by the National Science Foundation (NSF), Arlington, VA, under Award CBET-0933335. *Asterisk indicates corresponding author*.

C. B. Arena and M. B. Sano are with the Virginia Tech-Wake Forest School of Biomedical Engineering and Sciences, Bioelectromechanical Systems Laboratory, Virginia Polytechnic Institute and State University, Blacksburg, VA 24061 USA (e-mail: carena@vt.edu; sano@vt.edu).

M. N. Rylander is with the Virginia Tech-Wake Forest School of Biomedical Engineering and Sciences and the Virginia Tech Department of Mechanical Engineering, Bioheat Transfer and Nanotherapeutics Laboratory, Virginia Polytechnic Institute and State University, Blacksburg, VA 24061 USA (e-mail: mnr@vt.edu).

*R. V. Davalos is with the Virginia Tech-Wake Forest School of Biomedical Engineering and Sciences, Bioelectromechanical Systems Laboratory, Virginia Polytechnic and State University, Blacksburg, VA 24061 USA (e-mail: davalos@vt.edu).

Digital Object Identifier 10.1109/TBME.2010.2102021

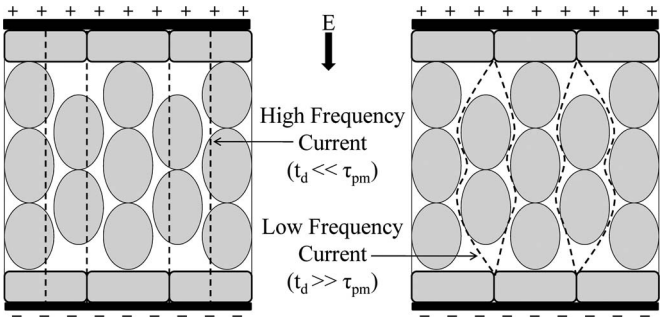

Fig. 1. Illustration of current pathways through epithelial layers and bulk tissue prior to the onset of electroporation. When the pulse duration t_d is much less than the plasma membrane time constant $\tau_{\rm pm}$, current flows through both intracellular and extracellular spaces (left). In the case that t_d is much more than $\tau_{\rm pm}$, current flow is restricted to the narrower extracellular spaces (right).

the dependence of electroporation on cell size, allowing more cells to be electroporated [24], [25]. In general, pore formation increases as long as the TMP is sustained above a critical threshold (∼1 V) [20]. One potential drawback of bipolar pulses is that they require higher field strengths to induce a given TMP as compared to a unipolar pulse of equivalent duration. This is apparent when the frequency of the bipolar pulses is increased, because the time interval above the critical TMP is reduced [25]. Kotnik *et al*. have explored the benefits of bipolar pulse trains at significantly lower frequencies, up to 1 kHz (i.e., 500 μs duration of single polarity). At lower frequencies, theoretical results show that the pore formation asymmetry can also be normalized with bipolar pulses [26]. Experimentally, bipolar pulses reduce electrolytic contamination [27] and the required field strength for reversible electroporation, while the field strength required for IRE remains unchanged [26]. The authors attribute this to the fact that when the duration of single polarity is much longer than the plasma membrane charging time, permeabilized area differences on the membrane between unipolar and bipolar pulses decreases as pulse amplitude increases.

Here, the benefits of high-frequency bipolar pulses for electroporation of tissue enclosed by an epithelium are studied. Epithelial layers containing tight junctions are preferred sites of electroporation for pulses with duration on the order of microseconds [28], [29]. This has to do with the fact that the electric current associated with pulses longer than the charging time of the plasma membrane (∼1 μs) [20] is confined to narrow, high-resistance extracellular spaces prior to the onset of electroporation (see Fig. 1) [30], [31]. It is possible for the field to penetrate epithelial layers when nanosecond pulsed electric field are employed, because current can flow through both extracellular and intracellular spaces [29], [31]. In this case, all cells present in the organ, regardless of their packing and morphology, experience a macroscopically homogeneous electric field distribution [32] (microscopic nonuniformities in the electric field are still present due to the packing of individual cells comprising the tissue). Therefore, high-frequency bipolar pulses with a duration of single polarity on the order of nanoseconds can be applied to treat tissue layers underlying the skin (see Fig. 2). Further, because the field is not concentrated across

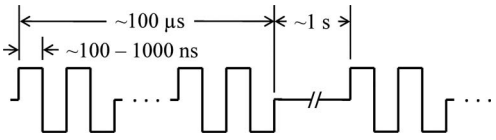

Fig. 2. Typical pulsing protocol for the proposed electroporation-based therapy. The total burst width of the high-frequency pulses (∼100 to 1000 ns duration of single polarity) is on the order of hundreds of microseconds, the time delay in between bursts is on the order of seconds, and the total number of bursts can be adjusted.

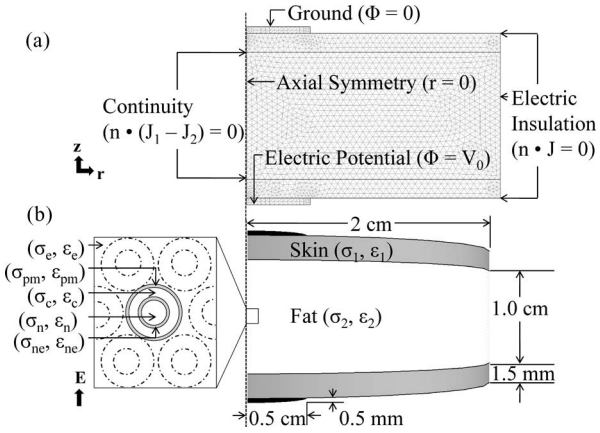

Fig. 3. (a) Meshed geometry of the FEM with boundary settings. The mesh consists of 3028 elements and was refined until there was $< 0.1\%$ change in the magnitude of the electric field at the center of the tissue. (b) Schematic diagram of the geometry with dimensions. The box represents an expanded view of the tissue that describes the link between the macroscopic electric field *E* and the microscopic analysis of TMP. Adjacent cells are drawn with dashed lines, indicating that their role was ignored in calculating TMP.

the epithelial cells, the potential for thermal damage in the skin should be reduced.

To quantify these apparent benefits, a finite element model (FEM) simulating plate electrodes surrounding a cylindrical tissue section through the center of a skin fold was constructed. Electroporation is often used to treat tumors that arise in fat tissue lying close to the skin [33]. The FEM incorporates physics for determining the electric field and temperature distribution within the heterogeneous system. Additionally, the electric field data generated were substituted into analytical calculations of TMP in order to determine the relationships between the pulse frequency and the extent of electroporation in the different tissue layers.

II. Methods

A 2-D axisymmetric FEM representative of a cylindrical section of noninfiltrated fat encapsulated by dry skin (see Fig. 3) was simulated using COMSOL 3.5a (Burlington, MA). The electric potential distribution within the tissue was obtained by transiently solving

$$-\nabla \cdot (\sigma \nabla \Phi) - \varepsilon_0 \varepsilon_r \nabla \cdot \left(\frac{\partial \nabla \Phi}{\partial t} \right) = 0 \qquad (1)$$

where Φ is the electric potential and σ and ε_r are the conductivity and relative permittivity of each tissue layer, respectively, which

TABLE I
DIELECTRIC PROPERTIES OF THE FEM SIMULATION DOMAIN

Frequency (Pulse Duration)	Waveform	Property	Tissue	
			Skin	Fat
250 kHz (2 μs)	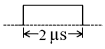	σ (S/m)	0.00216	0.0263
		ε_r	888	47
500 kHz (1 μs (×2))		σ (S/m)	0.00485	0.0265
		ε_r	851	33
1 MHz (500 ns (×4))	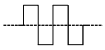	σ (S/m)	0.0119	0.0267
		ε_r	792	25
2 MHz (250 ns (×8))	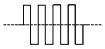	σ (S/m)	0.0290	0.0270
		ε_r	700	20

TABLE II
THERMAL PROPERTIES OF THE FEM SIMULATION DOMAIN

Property	Tissue		
	Blood	Skin	Fat
ρ (kg/m^3)	1069	1085	850
C (J/(kg·K))	3650	3680	2300
k (W/(m·K))	-	0.47	0.16
ω_b(1/s)	-	1.1	0.0036
Q_m (W/m^3)	-	368	58

depends on frequency (see Table I). Equation (1) is obtained from Maxwell's equations assuming no external current density (current density $J = \sigma E$), no remnant displacement (electric displacement $D = \varepsilon_0 \varepsilon_r E$), and the electro-quasistatic approximation. This approximation neglects magnetic induction ($\nabla \times E = 0$), which allows for the expression of the electric field only in terms of the electric potential:

$$E = -\nabla \Phi. \tag{2}$$

The dielectric properties of the bulk tissue were chosen from the data generated by Gabriel *et al*. [34] available online (http://niremf.ifac.cnr.it/docs/dielectric/home.html). The data were interpolated in Mathematica 7 (Wolfram Research, Inc., Champaign, IL) in order to estimate the dielectric properties at the desired frequencies. Dielectric properties of the electrode were chosen to be stainless steel, as incorporated in the Comsol material library. All electrical boundary conditions are shown in Fig. 3.

Because rectangular waveforms are comprised of components with various frequencies and amplitudes, tissue properties at frequencies associated with the carrier frequency, defined as the inverse of twice the duration of single polarity, are chosen. Intuitively, the duration of single polarity defines the frequency at which the current changes direction in the tissue. The pulses were constructed by multiplying the applied voltage by a function consisting of two smoothed Heaviside functions with a continuous second derivative and a tolerance of 5 ns (rise and fall times). The electro-quasistatic assumption is confirmed based on the fact that the primary frequency of the pulses is lower than 200 MHz (rise and fall times), which corresponds to a wavelength and skin depth that is greater than the longest dimension in the geometry [35]. The inclusion of a permittivity term in (1) differs from previous, simplified models [36], [37], and accounts for the reactive component of tissue to time-dependent pulsing, which is required for obtaining accurate potential distributions in heterogeneous models [38].

The temperature distribution in the tissue was obtained by transiently solving a modified version of the Pennes bioheat equation [39] with the inclusion of a Joule heating term:

$$\rho C \frac{\partial T}{\partial t} = \nabla \cdot (k \nabla T) + \rho_b \omega_b C_b (T_b - T) + Q_m + |J \cdot E| \tag{3}$$

where T is the tissue temperature, T_b is the blood temperature, k is the thermal conductivity of the tissue, C and C_b are the tissue and blood specific heat, respectively, ρ and ρ_b are the tissue and blood density, respectively, Q_m is the metabolic heat source term, ω_b is the blood perfusion coefficient, and $|J \cdot E|$ is the Joule heating term. All thermal tissue properties are given in Table II [40]. Due to the presence of different tissue layers and the high frequencies under consideration (250 kHz to 2 MHz), displacement currents are considered along with conduction currents in the formulation of Joule heating

$$J = J_D + J_C = \varepsilon_0 \varepsilon_r \frac{\partial E}{\partial t} + \sigma E \tag{4}$$

where J is the total current density, J_D is the displacement current density, and J_C is the conduction current density. In order to ensure that negative current components due to polarity changes add to the total current in the tissue, the absolute value of the resistive heating term was taken prior to temperature calculations. It was assumed that all subdomains were initially at physiologic temperature ($T_0 = 310.15$ K). The boundaries between the electrode–skin interface and the skin–fat interface were treated as continuous [$n \cdot (k_1 \nabla T_1 - k_2 \nabla T_2) = 0$], the centerline was defined as axial symmetry ($r = 0$), and the remaining boundaries were thermally insulated [$n \cdot (k \nabla T) = 0$] for conservative temperature estimates. Temperature profiles were investigated along the centerline ($r = 0$ mm) in the middle of the fat ($z = 0$ mm) and skin ($z = 5.75$ mm) layers. Data were imported into Mathematica, and a moving average with a period of 100 ns was taken to smooth the plots. Additionally, the data were fit with a linear trendline in order to extrapolate to longer burst widths and predict the onset of thermal damage.

By treating cells as a series of spherical, dielectric shells containing and surrounded by a conductive medium, the analytical solution for induced TMP across the plasma membrane ($\Delta \Phi$) can be obtained according to the law of total current [41]:

$$\nabla \cdot \left(\varepsilon_0 \varepsilon_r \frac{\partial E}{\partial t} + \sigma E \right) = \Lambda_k \nabla \cdot E = 0 \tag{5}$$

$$\Lambda_k = \sigma + \varepsilon_0 \varepsilon_r \frac{\partial}{\partial t} \tag{6}$$

where Λ is the admittivity operator and the subscript k denotes cellular regions including the nucleoplasm n, nuclear envelope

TABLE III
DIELECTRIC PROPERTIES OF ANALYTICAL TMP CALCULATION

Region	σ (S/m)	ε_r	Dimensions (m)
Extracellular Space	0.6	80.0	-
Plasma Membrane	5.3×10^{-6}	7.0	7.0×10^{-9} (thickness)
Cytoplasm	0.13	60.0	5.0×10^{-6} (radius)
Nuclear Envelope	4.3×10^{-3}	22.8	40.0×10^{-9} (thickness)
Nucleoplasm	0.18	120.0	2.5×10^{-6} (radius)

ne, cytoplasm *c*, plasma membrane *pm*, and extracellular space *e*. Transforming (2), (5), and (6) into the frequency domain [41]

$$E = -\nabla\Phi(s) \tag{7}$$

$$\Lambda_k \nabla \cdot E(s) = 0 \tag{8}$$

$$\Lambda_k(s) = \sigma + \varepsilon_0 \varepsilon_r s \tag{9}$$

where $s = j\omega = j2\pi f$, and applying the appropriate boundary conditions of potential continuity and normal vector continuity of current density at the interface between the different regions yields the solution for TMP [41]

$$\Delta\Phi(s) = F(\Lambda_n, \Lambda_{\rm ne}, \Lambda_c, \Lambda_{\rm pm}, \Lambda_e) E(s) \cos\theta \tag{10}$$

where θ represents the polar angle at the cell center between the electric field and the point of interest along the membrane. TMP is defined as the potential directly outside the membrane minus the inside. The natural, resting component of the plasma membrane TMP was ignored in all simulations, because it is typically an order of magnitude less than the induced TMP [20]. Further, the TMP across the nuclear envelope never reached a permeabilizing threshold with the chosen pulsing protocols, and reference to TMP from this point forward refers only to the plasma membrane. The term $F(\Lambda_k)$ represents a transfer function of the TMP that reflects the geometric and dielectric properties of the cellular regions (see Table III) [42] as a function of the admittivity. Dielectric properties at the cellular level are assumed to be frequency independent, which is valid for predicting TMP up to ~100 MHz [43]. The exact formulation for $F(\Lambda_k)$ is lengthy and can be found in [44], but is not included here for brevity. The term *E(s)* represents the Laplace transform of the pulsed electric field as a function of time.

The analytical model was utilized in two instances. In the first scenario, the frequency dependence of the induced TMP was investigated. Both rectangular and sinusoidal electric fields with identical maximum amplitude were compared. Rectangular waveforms were constructed with a series of step functions (ideal rise time) of alternating polarity and duration, and sinusoidal waveforms were constructed with a single sine function of varying frequency. The electric fields were substituted into (10), and the equations were solved directly in Mathematica.

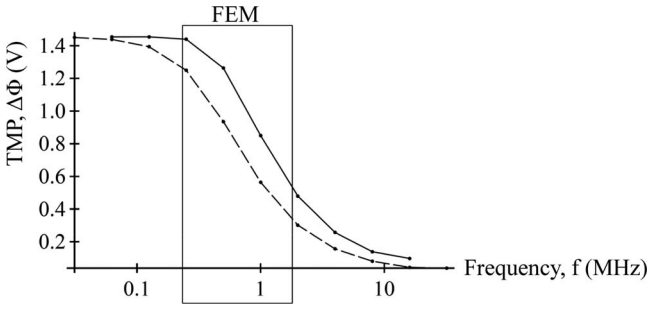

Fig. 4. Frequency *f* response of the TMP at the cell pole ($\theta = 0$) for rectangular bipolar pulses (–) and sinusoidal waveforms (– –). The box illustrates the frequency window implemented in the FEM.

This analysis provided insight as to which pulse waveforms and frequencies should be simulated by the FEM.

In the second case, TMP profiles were investigated around a hypothetical cell located along the centerline ($r = 0$ mm) in the middle of the fat ($z = 0$) and skin ($z = 5.75$ mm) layers of the FEM. The equations for TMP are derived under the assumption that there is no influence on the microscopic electric field from neighboring cells. Therefore, the macroscopic electric field in the bulk tissue predicted by the FEM dictates the microscopic electric field experienced by the cell. The vertical *z*-component of the electric field was imported from specific locations within the FEM into Mathematica to account for polarity changes. The radial *r*-component was neglected due to the fact that it never surpassed 3 V/cm as a current traveled primarily in the *z*-direction. Nonuniform electric field data were fit with a series of step functions (50-ns duration), such that the Laplace transform of the field could be performed and the solution for TMP could be obtained in the frequency domain as the summation of individual steps. The inverse Laplace transform of the data was then taken to obtain the complete time courses.

III. RESULTS

Results of the parametric study on TMP for frequencies spanning from 62.5 kHz to 16 MHz are shown in Fig. 4. The maximum amplitude of the sinusoidal and bipolar rectangular electric fields was 2000 V/cm (peak). For this applied field and the given geometric and dielectric properties of the modeled cell, the TMP never exceeds 1.46 V. Additionally, the time constant of the plasma membrane is 345 ns. All measurements were taken at the cell pole ($\theta = 0$) to depict the maximum achieved TMP after the system reached a steady oscillatory state. From the curve, as the frequency increases, the magnitude of the TMP is reduced. For the sinusoidal waveform, the reduction is evident at lower frequencies compared to the rectangular waveform. This has to do with the fact that the rectangular waveform maintains its maximum amplitude for a longer period of time than the sinusoidal waveform. It is not until the frequency of the rectangular waveform surpasses 250 kHz that a dramatic decrease in TMP occurs. For this reason, only rectangular pulses in a frequency window of 250 kHz to 2 MHz were investigated in the FEM, since they are best suited for electroporation with high-frequency bipolar pulses.

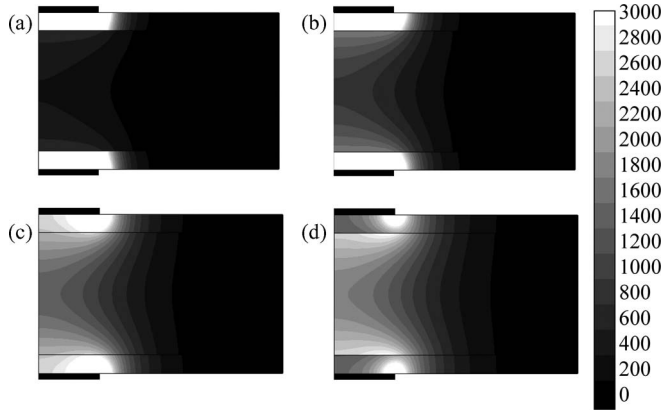

Fig. 5. Electric field, norm (V/cm) contours predicted by the FEM at the end of a 2-μs burst with an amplitude of 2600 V and a frequency of (a) 250 kHz, (b) 500 kHz, (c) 1 MHz, and (d) 2 MHz.

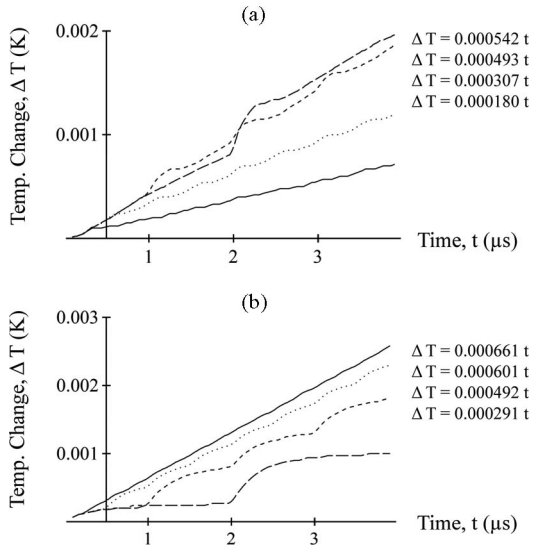

Fig. 6. Temperature changes predicted by the FEM at the center of the (a) skin and (b) fat for frequencies of 250 kHz (——), 500 kHz (- - -), 1 MHz (· · ·), and 2 MHz (–). Equations represent a linear fit to the data.

Fig. 5 shows the electric field distribution at the end of a 2-μs burst with various frequencies given in Table I. In each case, the maximum applied voltage was set to 2600 V (peak) in order to set up a voltage to distance ratio of 2000 V/cm between the electrodes (1.3-cm spacing). From the surface contour map, as frequency is increased, the electric field in the fat rises while the field in the skin drops. This trend extends to the point that at 2 MHz the field in the skin is lower than the fat, which is a direct result of the tissue dielectric properties at that frequency (greater conductivity and permittivity of skin as compared to fat). Therefore, high-frequency fields, are better suited to penetrate epithelial layers, such as the skin, and reach underlying tissue.

Temperature changes predicted by the FEM at the center of the skin and fat are shown in Fig. 6. In this case, a burst width of 4 μs was simulated in order to capture the trends in temperature development. Polarity of the 2-μs pulse (250 kHz) was switched between pulses to maintain consistency with the

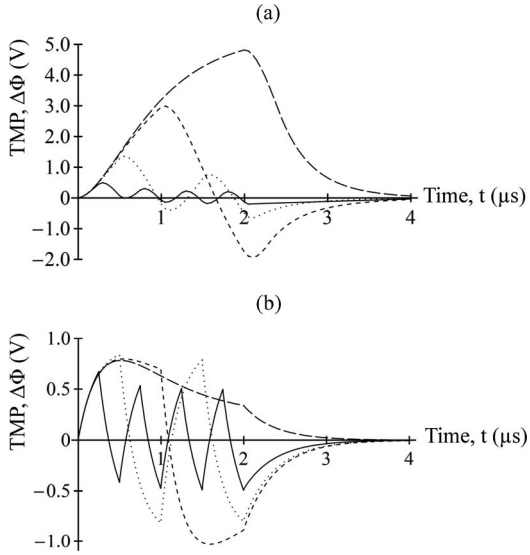

Fig. 7. TMP predicted by the FEM at the center of the (a) skin and (b) fat for frequencies of 250 kHz (——), 500 kHz (- – -), 1 MHz (· · ·), and 2 MHz (–).

other waveforms that are inherently bipolar. With respect to the skin, as the frequency of the applied field increases, the temperature rises at a slower rate. This is a consequence of the fact that the electric field within the skin also decreases with increasing frequency. In the case of the fat, the temperature rises at a faster rate when the frequency of the applied field is increased. At first glance, this seems to be detrimental; however, it is merely an indication that energy is preferentially being deposited into the fat at higher frequencies. Again, this can be correlated with the electric field profile. In both tissues, the sharp rises in temperature are due to the spikes in displacement current that occur at the onset and offset of each pulse (data not shown). The total temperature increase in all cases is less than 0.003 K for a burst width of 4 μs. As explained in Section IV, even for bursts of longer widths, the temperature increase is not enough to promote thermal damage.

TMP profiles as predicted by the FEM on a hypothetical cell at the center of the skin and fat for a 2-μs burst width are shown in Fig. 7. All measurements were taken at the pole ($\theta = 0$) to depict the maximum induced TMP around the cell. With respect to the skin, as the frequency of the applied field increases, the maximum oscillation amplitude of the TMP decreases. This occurs for two reasons. First, as seen in Fig. 5, the electric field in the skin decreases with increasing frequency. Second, as seen in Fig. 4, even with constant field amplitude, the TMP decreases with increasing frequency, because the time during which the membrane has to charge before the polarity switches is less at higher frequencies. In the case of the fat, the behavior is slightly more complex. At lower frequencies, a majority of the voltage drop occurs across the skin, resulting in a reduced electric field in the fat. This shielding effect is best shown in Fig. 7 along the 250-kHz trace. According to Fig. 4, at 250 kHz, the maximum TMP should be reached. However, due to the shielding effect from the skin, a reduction in the TMP prior to the polarity change is seen. This reduction in TMP can be alleviated by increasing the frequency of the applied field. However, the

TABLE IV
PULSE FREQUENCY–TMP COMPARISON IN THE FAT LAYER

Frequency (pulse duration)	Time (μs), |TMP| > 0.5 (V)	% of Pulse, |TMP| > 0.5 (V)
250 kHz (2 μs)	1.2	60
500 kHz (1 μs (×2))	1.9	95
1 MHz (500 ns (×4))	1.3	65
2 MHz (250 ns (×8))	0.1	5

tradeoff between increased frequency and reduced TMP is still evident at a frequency of 2 MHz (250-ns pulse duration).

IV. DISCUSSION

As mentioned, electric current associated with pulses longer than $\sim$1 μs is confined to extracellular spaces prior to the onset of electroporation (see Fig. 1) [30], [31]. This can be attributed to the migration of charges toward biological membranes following the application of an external electric field. The time required for a membrane to become charged to 63% of its steady-state value is defined as the charging time constant of the membrane τ_{pm}. Based on the analytical model for TMP in this study, the time constant of the plasma membrane for a constant field is 345 ns. Additionally, steady state is not reached until after 1 μs. Displacement currents across the plasma membrane allow organelles to be exposed to fields during the time that it takes the plasma membrane to reach steady state [32]. Once steady state is achieved, the counterfield developed along the plasma membrane due to the accumulation of charges is significant enough to shield the field from entering the cell, and current is directed through extracellular spaces. Only after permeabilization of the membrane does ionic conduction allow the field to re-enter the cell [45]. If extracellular current pathways between cells are reduced, as in layers of epithelial cells connected by tight junctions [19], the field is highly concentrated across the layer, and the extent of electroporation in underlying cells is reduced.

There is a balance between employing pulses that are delivered on a short enough timescale to flow through epithelial cells but are long enough to induce electroporation in underlying cells. The time constant of 345 ns falls between the 2 MHz (250-ns pulse duration) and 1 MHz (500-ns pulse duration) bursts. Further, the 500-kHz burst (1-μs pulse duration) is close to the time it takes the TMP to reach steady state. Table IV summarizes the results based on the time that the TMP on a hypothetical cell at the center of the fat layer is above 0.5 V. This amplitude was chosen such that even the highest frequency burst was above the set voltage level for a certain amount of time. The results would hold if the applied field was doubled and the voltage level was set to the 1-V threshold for pore formation, due to the linear dependence of TMP on the electric field. Based on this criterion, a frequency of 500 kHz is best suited to treat cells in the fat layer, followed by 1 MHz and 250 kHz. As frequency is increased, the dielectric properties and electric field distribution in the skin and fat become more macroscopically homogeneous, but above 1 MHz, the pulse duration is not adequate for the cell to charge.

According to *in vitro* experiments that utilize bipolar rectangular pulses, the typical burst width required to induce either reversible electroporation or IRE increases with the frequency of the applied field. For EGT, a 60-kHz bipolar square wave with a burst width of 400 μs and an amplitude of 1600 V/cm has a six times greater transfection efficiency than a 1-MHz bipolar square wave with equal amplitude and width [22]. In terms of IRE, a 60-kHz bipolar square wave with a burst width of 400 μs and an amplitude of 4000 V/cm results in 19% cell viability [22]. These results were obtained when a single burst was delivered to the sample, and we were unable to find any data on high-frequency electroporation with rectangular pulses that implemented multiple bursts. Similar to how multiple unipolar pulses are typically delivered in ECT, EGT, or IRE protocols to enhance the desired outcome [46], [47], multiple bipolar bursts would likely produce similar trends. Data are also available for burst sinusoidal waveforms in the frequency range of 2 kHz to 50 MHz [48], [49], but the results are inconclusive, and sinusoidal waveforms are less efficient than rectangular bipolar pulses for inducing electroporation [50].

The onset of protein denaturation and loss of cell structure occur above 318.15 K [51], which correlates with an increase in temperature of 8 K above physiological temperature. Using this information, we can calculate the maximum energy delivery period (number of pulses multiplied by pulse duration) for an amplitude of 2000 V/cm at each of the frequencies investigated using the trendlines generated by the FEM data (see Fig. 6). In the skin layer, heating is reduced by increasing the frequency of the applied field. This confirms our initial hypothesis that the potential for thermal damage in the skin is reduced when the frequency of the applied field is increased. At higher frequencies, the energy is preferentially deposited in the fat layer. For 2 MHz, the total energy delivery period required to cause an 8-K increase in temperature is 12 ms. An example treatment plan would then be 12, 1-ms bursts separated by a delay of 1 s. If the frequency is reduced to 500 kHz, which shows the greatest electroporation efficiency (see Table IV), the allowable energy delivery period increases to 16 ms, which would permit the delivery of an additional 4, 1-ms bursts before the onset of thermal damage. The restrictions could be increased if less conservative estimates are obtained that account for heat dissipation between pulses and heat convection at the tissue surface [52]. These projected protocols represent a maximum, and it is likely that the desired effects will be induced at a significantly lower energy [46], [47].

This work has been geared toward developing a better way to deposit electrical energy through the skin, but similar structures are seen in underlying tissue layers. For example, pancreatic ducts are lined by epithelial cells that can give rise to tumors, and tumors of the breast are often surrounded by fatty tissue [53]. These features will play an important role in how the electric field is distributed within the tissue. This complicates treatment planning, where the goal is to predict the electric field distribution in the tissue in order to select an appropriate pulsing protocol. A benefit of high-frequency bursts with nanosecond-order pulses is their ability to penetrate tissue heterogeneities, resulting in more predictable treatment outcomes. These pulsing

protocols would then be useful if implemented not only with plate electrodes, but also with the alternative needle electrodes. Additionally, IRE treatments are often preceded by a nerve blocker or paralytic agent to minimize muscle contraction during treatment. *Ex vivo* muscle stimulation experiments indicate that the electric field threshold required to induce muscle contractions increases as the pulse duration decreases [54]. Therefore, the nanosecond-order pulses proposed here may allow the use of these paralytic agents to be averted.

Detailed geometric considerations, such as the individual tissue layers comprising the skin, layers of conductive gel used clinically to improve electrical contact, and the outer curvature of a typical skin fold, have been ignored in order to simplify our initial investigation. To be conservative in our estimates, dry skin was used in the model and the use of a conductive gel to wet the skin was not employed. The use of a gel and the properties of wet skin should further enhance the benefits of this technique. In this initial study, our goal was to elicit the benefit of high-frequency electroporation for overcoming impedance barriers without superimposing the effects from geometric intricacies and electroporation nonlinearities in the analysis. Future work should be directed toward expanding this focus.

In the analytical model for TMP, it was assumed that the electric field was applied across an isolated cell. In reality, tissues comprise a network of cells that create nonuniformities in the electric field at the microscopic level. In general, as the packing density of cells increases, the TMP decreases [55]. Thus, the overall trends presented here are valid, but the specific values for TMP should be scaled accordingly if the packing density is known. Additionally, dynamic dielectric tissue properties were neglected in both the analytical model and the FEM. At the macroscale, changes in tissue dielectric properties due to electroporation [14], [15] and temperature should be incorporated in the FEM. At the microscale, in order to prevent the development of unrealistic TMP in regions of high electric field, as seen here in the skin layer, the analytical calculation of TMP could be supplemented with equations for pore formation. Pores allow current to flow through the membrane, which limits the increase in TMP [23]–[25].

V. Conclusion

Our results indicate that bursts of bipolar, nanosecond pulses can maintain a critical TMP beneath epithelial layers, while minimizing heating in the epithelial layer. This has to do with the ability of nanosecond pulses to achieve a macroscopically homogeneous field distribution in a heterogeneous system. At high frequencies, tissues with a low passive DC conductivity become more conductive. This has implications not only for skin, as presented here, but also for other tissues, such as bone and lung. Experimental work needs to be conducted to optimize the total burst width, time between bursts, and total number of bursts required for inducing electroporation with high-frequency rectangular pulses. This study serves as the first step in assessing the feasibility of implementing high-frequency bipolar pulses for tissue electroporation. Based on the theoretical analysis presented here, the predicted benefits of high-frequency electroporation will translate experimentally to enhance the efficacy of ECT, EGT, or IRE for treating electrically isolated tumors, such as those encapsulated by the skin, pancreas, breast, bone, or lung.

Acknowledgment

The authors would like to thank P. A. Garcia for his expertise in modeling with Comsol, J. L. Caldwell for his knowledge on high-frequency electronics, and G. S. Brown, R. E. Neal II, and S. L. Matrangola for their general support.

References

[1] J. C. Weaver and Y. A. Chizmadzhev, "Theory of electroporation: A review," *Bioelectrochem. Bioener.*, VA, vol. 41, pp. 135–160, Dec. 1996.
[2] I. G. Abidor, V. B. Arakelyan, L. V. Chernomordik, Y. A. Chizmadzhev, V. F. Pastushenko, and M. P. Tarasevich, "Electric breakdown of bilayer lipid-membranes 1. Main experimental facts and their qualitative discussion," *Bioelectrochem. Bioenerg.*, vol. 6, pp. 37–52, 1979.
[3] R. Benz, F. Beckers, and U. Zimmermann, "Reversible electrical breakdown of lipid bilayer membranes: A charge-pulse relaxation study," *J. Membr. Biol.*, vol. 48, pp. 181–204, Jul. 16, 1979.
[4] E. Neumann and K. Rosenheck, "Permeability changes induced by electric impulses in vesicular membranes," *J. Membr. Biol.*, vol. 10, pp. 279–90, Dec. 29, 1972.
[5] J. Teissie and T. Y. Tsong, "Electric-field induced transient pores in phospholipid-bilayer vesicles," *Biochem.*, vol. 20, pp. 1548–1554, 1981.
[6] U. Zimmermann, G. Pilwat, and F. Riemann, "Dielectric breakdown of cell membranes," *Biophys. J*, vol. 14, pp. 881–899, Nov. 1974.
[7] K. Kinosita and T. Y. Tsong, "Formation and resealing of pores of controlled sizes in human erythrocyte-membrane," *Nature*, vol. 268, pp. 438–441, 1977.
[8] T. K. Wong and E. Neumann, "Electric field mediated gene transfer," *Biochem. Biophys. Res. Commun.*, vol. 107, pp. 584–587, Jul. 30, 1982.
[9] B. Rubinsky, "Irreversible electroporation in medicine," *Technol. Cancer Res. Treat.*, vol. 6, pp. 255–260, Aug. 2007.
[10] R. V. Davalos and B. Rubinsky, "Temperature considerations during irreversible electroporation," *Int. J. Heat Mass Transfer*, vol. 51, pp. 5617–5622, Nov. 2008.
[11] L. M. Mir and S. Orlowski, "Mechanisms of electrochemotherapy," *Adv. Drug Deliv. Rev.*, vol. 35, pp. 107–118, Jan. 4, 1999.
[12] R. V. Davalos, L. M. Mir, and B. Rubinsky, "Tissue ablation with irreversible electroporation," *Ann. Biomed. Eng.*, vol. 33, pp. 223–231, Feb. 2005.
[13] R. Nuccitelli, X. Chen, A. G. Pakhomov, W. H. Baldwin, S. Sheikh, J. L. Pomicter, W. Ren, C. Osgood, R. J. Swanson, J. F. Kolb, S. J. Beebe, and K. H. Schoenbach, "A new pulsed electric field therapy for melanoma disrupts the tumor's blood supply and causes complete remission without recurrence," *Int. J. Cancer*, vol. 125, pp. 438–45, Jul. 15, 2009.
[14] N. Pavselj, V. Preat, and D. Miklavcic, "A numerical model of skin electroporation as a method to enhance gene transfection in skin," in *Proc. 11th Mediterranean Conf. Med. Biol. Eng. Comput.*, 2007, vol. 16, pp. 597–601.
[15] N. Pavselj, Z. Bregar, D. Cukjati, D. Batiuskaite, L. M. Mir, and D. Miklavcic, "The course of tissue permeabilization studied on a mathematical model of a subcutaneous tumor in small animals," *IEEE Trans. Biomed. Eng.*, vol. 52, no. 8, pp. 1373–1381, Aug. 2005.
[16] T. Lamsa, H. Jin, J. Mikkonen, J. Laukkarinen, J. Sand, and I. Nordback, "Biocompatibility of a new bioabsorbable radiopaque stent material ($BaSO_4$ containing poly-LD-lactide) in the rat pancreas," *Pancreatology*, vol. 6, pp. 301–305, 2006.
[17] T. Lämsä, H. Jin, P. H. Nordback, J. Sand, T. Luukkaala, and I. Nordback, "Pancreatic Injury Response is Different Depending on the Method of Resecting the Parenchyma," *J. Surgical Res.*, vol. 154, no. 2, pp. 203–211, 2009.
[18] R. C. Lee and R. D. Astumian, "The physicochemical basis for thermal and non-thermal 'burn' injuries," *Burns*, vol. 22, pp. 509–519, Nov. 1996.
[19] D. M. Jones, R. H. Smallwood, D. R. Hose, B. H. Brown, and D. C. Walker, "Modelling of epithelial tissue impedance measured using three different designs of probe," *Physiol. Meas.*, vol. 24, pp. 605–623, May 2003.
[20] T. R. Gowrishankar, A. T. Esser, Z. Vasilkoski, K. C. Smith, and J. C. Weaver, "Microdosimetry for conventional and supra-electroporation

in cells with organelles," *Biochem. Biophys. Res. Commun.*, vol. 341, pp. 1266–1276, Mar. 24, 2006.
[21] D. C. Chang, "Cell poration and cell-fusion using an oscillating electric-field," *Biophys. J.*, vol. 56, pp. 641–652, Oct. 1989.
[22] E. Tekle, R. D. Astumian, and P. B. Chock, "Electroporation by using bipolar oscillating electric-field—an improved method for DNA transfection of Nih 3t3 cells," *Proc. Nat. Acad. Sci. U.S.A.*, vol. 88, pp. 4230–4234, May 1991.
[23] S. Talele and P. Gaynor, "Non-linear time domain model of electropermeabilization: Response of a single cell to an arbitrary applied electric field," *J. Electrostatics*, vol. 65, pp. 775–784, Nov. 2007.
[24] S. Talele and P. Gaynor, "Non-linear time domain model of electropermeabilization: Effect of extracellular conductivity and applied electric field parameters," *J. Electrostatics*, vol. 66, pp. 328–334, May 2008.
[25] S. Talele, P. Gaynor, M. J. Cree, and J. van Ekeran, "Modelling single cell electroporation with bipolar pulse parameters and dynamic pore radii," *J. Electrostatics*, vol. 68, pp. 261–274, Jun. 2010.
[26] T. Kotnik, L. M. Mir, K. Flisar, M. Puc, and D. Miklavcic, "Cell membrane electropermeabilization by symmetrical bipolar rectangular pulses. Part I: Increased efficiency of permeabilization," *Bioelectrochemistry*, vol. 54, pp. 83–90, Aug. 2001.
[27] T. Kotnik, D. Miklavcic, and L. M. Mir, "Cell membrane electropermeabilization by symmetrical bipolar rectangular pulses. Part II. Reduced electrolytic contamination," *Bioelectrochemistry*, vol. 54, pp. 91–95, Aug. 2001.
[28] T. R. Gowrishankar, C. Stewart, and J. C. Weaver, "Electroporation of a multicellular system: Asymptotic model analysis," in *Proc. IEEE 26th Annu. Int. Conf. Eng. Med. Biol. Soc.*, 2004, vol. 26, pp. 5444–5446.
[29] T. R. Gowrishankar and J. C. Weaver, "An approach to electrical modeling of single and multiple cells," *Proc. Nat. Acad. Sci. U.S.A.*, vol. 100, pp. 3203–3208, Mar. 18, 2003.
[30] A. T. Esser, K. C. Smith, T. R. Gowrishankar, and J. C. Weaver, "Towards solid tumor treatment by irreversible electroporation: intrinsic redistribution of fields and currents in tissue," *Technol. Cancer Res. Treatment*, vol. 6, pp. 261–74, Aug. 2007.
[31] A. Ivorra, Ed.,,"Tissue Electroporation as a Bioelectric Phenomenon: Basic Concepts," Irreversible Electroporation. Berlin, Germany: Springer, 2010.
[32] A. T. Esser, K. C. Smith, T. R. Gowrishankar, and J. C. Weaver, "Towards Solid Tumor Treatment by Nanosecond Pulsed Electric Fields," *Technol. Cancer Res. Treatment*, vol. 8, pp. 289–306, Aug. 2009.
[33] L. M. Mir, P. Devauchelle, F. Quintin-Colonna, F. Delisle, S. Doliger, D. Fradelizi, J. Belehradek, and S. Orlowski, "First clinical trial of cat soft-tissue sarcomas treatment by electrochemotherapy," *Brit. J. Cancer*, vol. 76, pp. 1617–1622, Dec. 1997.
[34] S. Gabriel, R. W. Lau, and C. Gabriel, "The dielectric properties of biological tissues. 2. Measurements in the frequency range 10 Hz to 20 GHz," *Phys. Med. Biol.*, vol. 41, pp. 2251–2269, Nov. 1996.
[35] M. T. Chen, C. Jiang, P. T. Vernier, Y. H. Wu, and M. A. Gundersen, "Two-dimensional nanosecond electric field mapping based on cell electropermeabilization," *PMC Biophys.*, vol. 2, p. 9, 2009.
[36] J. F. Edd and R. V. Davalos, "Mathematical modeling of irreversible electroporation for treatment planning," *Technol. Cancer Res. Treatment*, vol. 6, pp. 275–286, Aug. 2007.
[37] R. E. Neal and R. V. Davalos, "The feasibility of irreversible electroporation for the treatment of breast cancer and other heterogeneous systems," *Ann. Biomed. Eng.*, vol. 37, pp. 2615–2625, Dec. 2009.
[38] N. Yousif, R. Bayford, and X. Liu, "The influence of reactivity of the electrode-brain interface on the crossing electric current in therapeutic deep brain stimulation," *Neuroscience*, vol. 156, pp. 597–606, Oct. 15, 2008.
[39] H. H. Pennes, "Analysis of tissue and arterial blood temperatures in the resting human forearm," *J. Appl. Physiol.*, vol. 1, pp. 93–122, Aug. 1948.
[40] D. Fiala, K. J. Lomas, and M. Stohrer, "A computer model of human thermoregulation for a wide range of environmental conditions: The passive system," *J. Appl. Physiol.*, vol. 87, pp. 1957–1972, Nov. 1999.
[41] C. G. Yao, D. B. Mo, C. X. Li, C. X. Sun, and Y. Mi, "Study of transmembrane potentials of inner and outer membranes induced by pulsed-electric-field model and simulation," *IEEE Trans. Plasma Sci.*, vol. 35, no. 5, pp. 1541–1549, Oct. 2007.
[42] Q. Hu, S. Viswanadham, R. P. Joshi, K. H. Schoenbach, S. J. Beebe, and P. F. Blackmore, "Simulations of transient membrane behavior in cells subjected to a high-intensity ultrashort electric pulse," *Phys. Rev. E*, vol. 71, no. 3, p. 031914, Mar. 2005.
[43] T. Kotnik and D. Miklavcic, "Theoretical evaluation of the distributed power dissipation in biological cells exposed to electric fields," *Bioelectromagn.*, vol. 21, pp. 385–394, Jul. 2000.
[44] T. Kotnik and D. Miklavcic, "Theoretical evaluation of voltage inducement on internal membranes of biological cells exposed to electric fields," *Biophys. J.*, vol. 90, pp. 480–491, Jan. 2006.
[45] J. F. Kolb, S. Kono, and K. H. Schoenbach, "Nanosecond pulsed electric field generators for the study of subcellular effects," *Bioelectromagn.*, vol. 27, pp. 172–187, Apr. 2006.
[46] J. Belehradek, S. Orlowski, L. H. Ramirez, G. Pron, B. Poddevin, and L. M. Mir, "Electropermeabilization of cells in tissues assessed by the qualitative and quantitative electroloading of bleomycin," *Biochimica Et Biophysica Acta-Biomembranes*, vol. 1190, pp. 155–163, Feb. 23, 1994.
[47] P. A. Garcia, J. H. Rossmeisl, R. E. Neal, T. L. Ellis, J. D. Olson, N. Henao-Guerrero, J. Robertson, and R. V. Davalos, "Intracranial nonthermal irreversible electroporation: *In vivo* analysis," *J. Membrane Biol.*, vol. 236, pp. 127–136, Jul. 2010.
[48] D. W. Jordan, R. M. Gilgenbach, M. D. Uhler, L. H. Gates, and Y. Y. Lau, "Effect of pulsed, high-power radiofrequency radiation on electroporation of mammalian cells," *IEEE Trans. Plasma Sci.*, vol. 32, no. 4, pp. 1573–1578, Aug. 2004.
[49] S. Katsuki, N. Nomura, H. Koga, H. Akiyama, I. Uchida, and S.-I. Abe, "Biological effects of narrow band pulsed electric fields," *IEEE Trans Dielectr. Electr. Insulat.*, vol. 14, no. 3, pp. 663–668, Jun. 2007.
[50] T. Kotnik, G. Pucihar, M. Rebersek, D. Miklavcic, and L. M. Mir, "Role of pulse shape in cell membrane electropermeabilization," *Biochimica Et Biophysica Acta-Biomembranes*, vol. 1614, pp. 193–200, Aug. 7, 2003.
[51] A. J. Bilchik, T. F. Wood, and D. P. Allegra, "Radiofrequency ablation of unresectable hepatic malignancies: Lessons learned," *Oncologist*, vol. 6, pp. 24–33, 2001.
[52] I. Lackovic, R. Magjarevic, and D. Miklavcic, "Three-dimensional finite-element analysis of joule heating in electrochemotherapy and in vivo ge," *IEEE Trans. Dielectr. Electr. Insul.*, vol. 16, no. 5, pp. 1338–1347, Oct. 2009.
[53] A. J. Surowiec, S. S. Stuchly, J. R. Barr, and A. Swarup, "Dielectric-properties of breast-carcinoma and the surrounding tissues," *IEEE Trans. Biomed. Eng.*, vol. 35, no. 4, pp. 257–263, Apr. 1988.
[54] W. R. Rogers, J. H. Merritt, J. A. Comeaux, C. T. Kuhnel, D. F. Moreland, D. G. Teltschik, J. H. Lucas, and M. R. Murphy, "Strength-duration curve for an electrically excitable tissue extended down to near 1 nanosecond," *IEEE Trans. Plasma Sci.*, vol. 32, no. 4, pp. 1587–1599, Aug. 2004.
[55] R. Susil, D. Semrov, and D. Miklavcic, "Electric field-induced transmembrane potential depends on cell density and organization," *Electro Magnetobiol.*, vol. 17, pp. 391–399, 1998.

Christopher B. Arena received the B.S. degree in biomedical engineering from the University of Virginia, Charlottesville, in 2008. He is a Graduate Student at the Virginia Tech-Wake Forest University School of Biomedical Engineering and Sciences.

He works in the Bioelectromechanical Systems Laboratory at Virginia Polytechnic Institute and State University, Blacksburg. His research interests include high frequency electroporation and irreversible electroporation combined with nanoparticles for cancer treatment.

Michael B. Sano received the B.S. degree in mathematics and electrical engineering from the University at Buffalo in 2007 and the M.S. degree in engineering mechanics from Virginia Polytechnic Institute and State University, Blacksburg. He is a Graduate Student at the Virginia Tech-Wake Forest University School of Biomedical Engineering and Sciences.

He works in the Bioelectromechanical Systems Laboratory at Virginia Polytechnic Institute and State University. His research interests include contactless dielectrophoresis and tissue decellularization with irreversible electroporation.

Marissa Nichole Rylander received the B.S. degree in 2000, M.S. degree in 2002, and the Ph.D. degree in 2005 from the University of Texas-Austin.

She is an Assistant Professor jointly appointed in the Virginia Tech - Wake Forest University School of Biomedical Engineering and Sciences and the Virginia Tech Department of Mechanical Engineering. She directs the Bioheat Transfer and Nanotherapeutics Laboratory at Virginia Tech. Her research interests include nanotechnology for therapeutics and heat shock protein expression in tumors.

Rafael V. Davalos (M'05) received the B.S. degree in 1994 from Cornell University, Ithaca, NY and the Ph.D. degree in 2002 from the University of California, Berkeley.

He is an Assistant Professor in the Virginia Tech - Wake Forest University School of Biomedical Engineering and Sciences. He directs the Bioelectromechanical Systems Laboratory and holds Adjunct Appointments at the Wake Forest Institute of Regenerative Medicine, the Wake Forest University Comprehensive Cancer Center, and the Virginia Tech Engineering Science and Mechanics Department.